

Article

Lower Limits of Petrophysical Properties Allowing Natural Gas Accumulation in Marine Sandstones: An Example from the Qiongdongnan Basin, Northern South China Sea

Chao Li ^{1,2}, Shuai Guo ³, Qianshan Zhou ^{1,2,*}, Chaochao Xu ^{1,4,*} and Guojun Chen ^{1,2}

¹ Northwest Institute of Eco-Environment and Resources, Chinese Academy of Sciences, Lanzhou 730000, China; lichaomails@lzb.ac.cn (C.L.); gjchen@lzb.ac.cn (G.C.)

² Key Laboratory of Petroleum Resources Exploration and Evaluation, Lanzhou 730000, China

³ Research Institute of China National Offshore Oil Corporation, Beijing 100028, China; guoshuai@cnooc.com.cn

⁴ University of Chinese Academy of Sciences, Beijing 100049, China

* Correspondence: zhouqianshan@nieer.ac.cn (Q.Z.); xuchaochao1998@163.com (C.X.)

Abstract: The lower limits of petrophysical properties for an effective reservoir are among the key parameters for assessing hydrocarbon reserves and are therefore directly related to hydrocarbon exploration and development strategies. However, the lower limits for marine sandstone gas reservoirs are still not clear and the impact factors also remain to be discussed. This study analysed the lower petrophysical property limits of an effective sandstone reservoir in the Qiongdongnan Basin using porosity, permeability and gas testing. The results showed that the lower porosity and permeability limits of effective reservoirs developed in the deltas are 8.9% and $1.2 \times 10^{-3} \mu\text{m}^2$, respectively, and 11.3% and $4.0 \times 10^{-3} \mu\text{m}^2$ in the submarine canyons and fans, respectively. Sedimentary facies, sediment transport distance, grain size and burial depth of sandstone significantly influence the lower physical property limits. The lower porosity and permeability limits increase with the increase in sediment transport distance as well as the decrease in sandstone grain size and burial depth. Sediment sources and sedimentary facies determine whether sandstone can become an effective reservoir in the Qiongdongnan Basin. Specifically, the sediment source dramatically influences the petrophysical properties of sandstone. The sandstone sourced from the Red River has higher porosity and permeability, followed by the sandstone sourced from the Hainan Uplift, and the sandstone sourced from the palaeo-uplift within the basin has the lowest porosity and permeability. The feldspar dissolution by CO₂ and organic acid is the primary formation mechanism of the effective reservoir in the Lingshui Formation, whereas the dissolution of glauconite is more common in the sandstone reservoirs of the Sanya and Meishan formations.

Keywords: effective reservoir; lower petrophysical properties limits; formation mechanism; Qiongdongnan Basin; South China Sea



Citation: Li, C.; Guo, S.; Zhou, Q.; Xu, C.; Chen, G. Lower Limits of Petrophysical Properties Allowing Natural Gas Accumulation in Marine Sandstones: An Example from the Qiongdongnan Basin, Northern South China Sea. *J. Mar. Sci. Eng.* **2024**, *12*, 735. <https://doi.org/10.3390/jmse12050735>

Academic Editor: Dimitris Sakellariou

Received: 28 March 2024

Revised: 25 April 2024

Accepted: 25 April 2024

Published: 28 April 2024



Copyright: © 2024 by the authors. Licensee MDPI, Basel, Switzerland. This article is an open access article distributed under the terms and conditions of the Creative Commons Attribution (CC BY) license (<https://creativecommons.org/licenses/by/4.0/>).

1. Introduction

Recently, tight oil or gas exploration has received increasing attention [1–6]. Due to the high technical requirements for tight oil or gas exploration, its use costs much more than conventional oil or gas [7–12]. Efficient tight oil or natural gas exploration is one way to reduce costs, making oil and gas explorers consider the lower physical property limits [13–17]. The definition of the lower limits of physical properties for effective reservoirs is the minimum porosity and minimum permeability required for fluid accumulation in rocks [13–15]. The lower porosity and permeability limits of the reservoirs have become fundamental factors for assessing oil or natural gas reserves; they are directly related to oil or natural gas exploration strategies [18–22]. Similarly, deepwater oil or gas exploration also faces this dilemma [23,24]. In addition to considering the buried depth of the reservoirs, offshore drilling pays attention to the current seawater depth because the requirements of deepwater

oil or gas exploration for drilling technology are far higher than those of shallow-water areas [23,24]. Deepwater oil or gas exploration costs much more than shallow-water oil or natural gas exploration [23–25]. Therefore, when exploring deepwater oil or natural gas, researchers must also consider the lower porosity and permeability limits of the reservoirs. However, the lower porosity and permeability limits of the reservoirs distributed in marine deepwater areas have rarely been studied.

Previous studies have determined the lower porosity and permeability limits of effective reservoirs using empirical statistics, oil testing, oil-bearing analysis and other methods [13–15,17,20,22,26–29]. The results show that the lower porosity and permeability limits of the tight sandstone of the Ordos, Junggar and Songliao basins, China, are 3–12% and $0.02\text{--}1 \times 10^{-3} \mu\text{m}^2$ [13–15,17,30]. Source rock, buried depth and hydrocarbon generation kinetics are the primary factors influencing the lower porosity and permeability limits of tight reservoirs [17,18,20,26,28,29,31–33]. The development and evolution of sandstone reservoirs are jointly controlled by the basin tectonic background, sedimentary facies, diagenesis, palaeoclimate, palaeotemperature and other factors [20,27,31–33]. The sedimentary facies forms the basis for reservoir development, and the later reconstruction of a reservoir formed by diagenesis is key to reservoir performance [20,31,33]. Pressure and cementation determine the degree of compaction of a reservoir, while dissolution is the key to the development of secondary pores in a reservoir [31,33]. Therefore, the sedimentary facies and diagenesis are vital for determining reservoir properties [20,31,33]. However, the effects of sedimentary facies, sediment transport distance and grain size on the lower porosity and permeability limits of effective reservoirs are yet to be discussed.

The objectives of this study were to (1) investigate the lower porosity and permeability limits of effective reservoir and its influence factors and (2) evaluate the roles of sediment source, sediment transport distance, sedimentary facies and dissolution diagenesis on the formation of an effective reservoir. The results are of practical significance for guiding the selection of natural gas exploration zones in the Qiongdongnan Basin (QDNB).

2. Geological Background

The QDNB is in the northern area of the South China Sea (see Figure 1A). NE-, NNE-, NW- and EW-trending faults controlled the development of the Songxi Sag (SXS), Songdong Sag (SDS), Yabei Sag (YBS), Yanan Sag (YNS) and Songtao Uplift (STU) in the northern depression; the Changchang Sag (CCS), Songnan–Baodao Sag (SN–BDS), Lingshui Sag (LSS), Ledong Sag (LDS) and Songnan Uplift (SNU) in the central depression and the Beijiao Sag (BJS) in the southern depression (see Figure 1B). The western QDNB contains YBS, YNS, LDS and LSS, and the eastern QDNB contains SXS, SDS, SN–BDS and CCS (see Figure 1B). The tectonic evolution of the QDNB includes the rifting (35–23 Ma) and post-rift subsidence stages (23–0 Ma) [34–36].

The QDNB is developed on Mesozoic basement and contains a thickness of 6000–12,000 m Tertiary to Quaternary sediments (see Figure 2) [37,38]. Rifting commenced in the Eocene and finished around the late Oligocene, leaving a series of sags that are filled with lacustrine sediments (see Figure 2) [37,38]. During the early Oligocene, the Yacheng Formation (YCF) comprised neritic and coastal-plain coal-bearing sediments (see Figure 2) [37,38]. Immediately above the Yacheng Formation is the littoral to neritic Lingshui Formation (LSF) (see Figure 2) [37,38]. Following the rifting stage, the QDNB experienced post-rift thermal subsidence to date and was filled with a thick sequence of marine sediments (see Figure 2) [37,38]. In the post-rift subsidence stage, marine sediments dominated by mudstones with occasional turbidite channels and deepwater fan sandstone were deposited in the Miocene Sanya Formation (SYF), Meishan Formation (MSF), Huangliu Formation (HLF) and the Pliocene Yinggehai Formation (YGHF) (see Figure 2) [37,38]. The primary strata in this study are the LSF, SYF and MSF.

The sediments source of the QDNB includes the palaeo-uplifts within the basin, the Hainan Uplift and the Red River [39–42]. These sediment sources were dominant in different periods [43]. The basin was in the rifting stage during the deposition of the YCF

and LSF, and each sag was an independent sedimentary unit [34–36]. The sediments of each sag during this period primarily originated from the palaeo-uplifts adjacent to the sag, and the transport distance of these sediments was short [41]. During the deposition of the Miocene SYF and MSF, the basin was in the post-rift subsidence stage, and the sediments from the Hainan Uplift entered the basin widely and occupied a dominant position [34,36,44]. The transport distance of these sediments is longer than that of the Oligocene sediments. During the late Miocene HLF and Pliocene YGHF depositions, the sediment transported by the Red River entered the basin and deposited as a large submarine fan and canyon with the longest transportation distance [42,45,46].

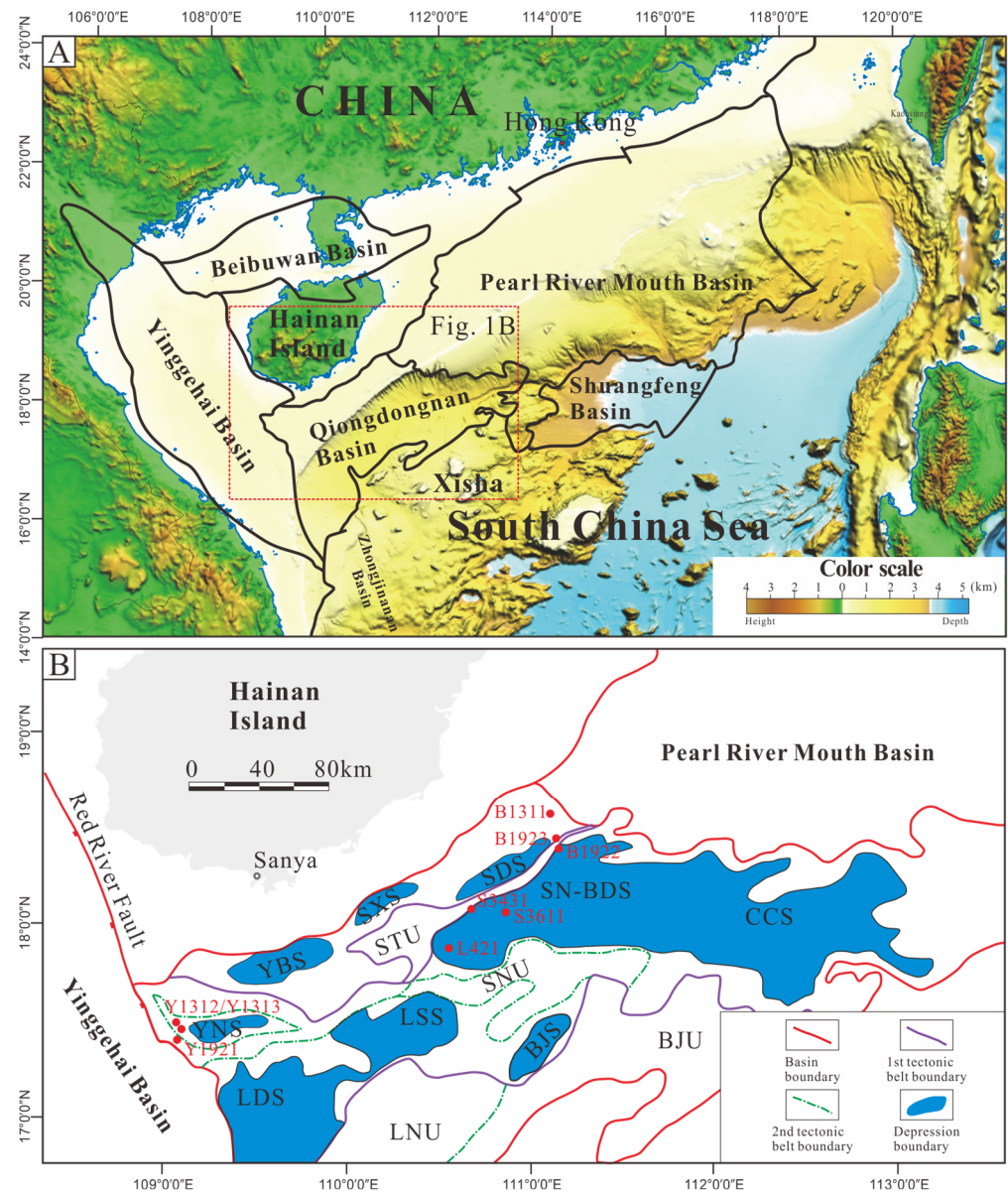


Figure 1. Map showing the location of the Qiongdongnan Basin (A) and the sags of the Qiongdongnan Basin (B). A 3D topographic map in (A), modified after Yang [47]. Legends: YBS: Yabei Sag; SXS: Songxi Sag; SDS: Songdong Sag; YNS: Yanan Sag; LDS: Ledong Sag; LSS: Lingshui Sag; SN–BDS: Songnan–Baodao Sag; CCS: Changchang Sag; BJS: Beijiao Sag; STU: Songtao Uplift; SNU: Songnan Uplift; LNU: Lingnan Uplift.

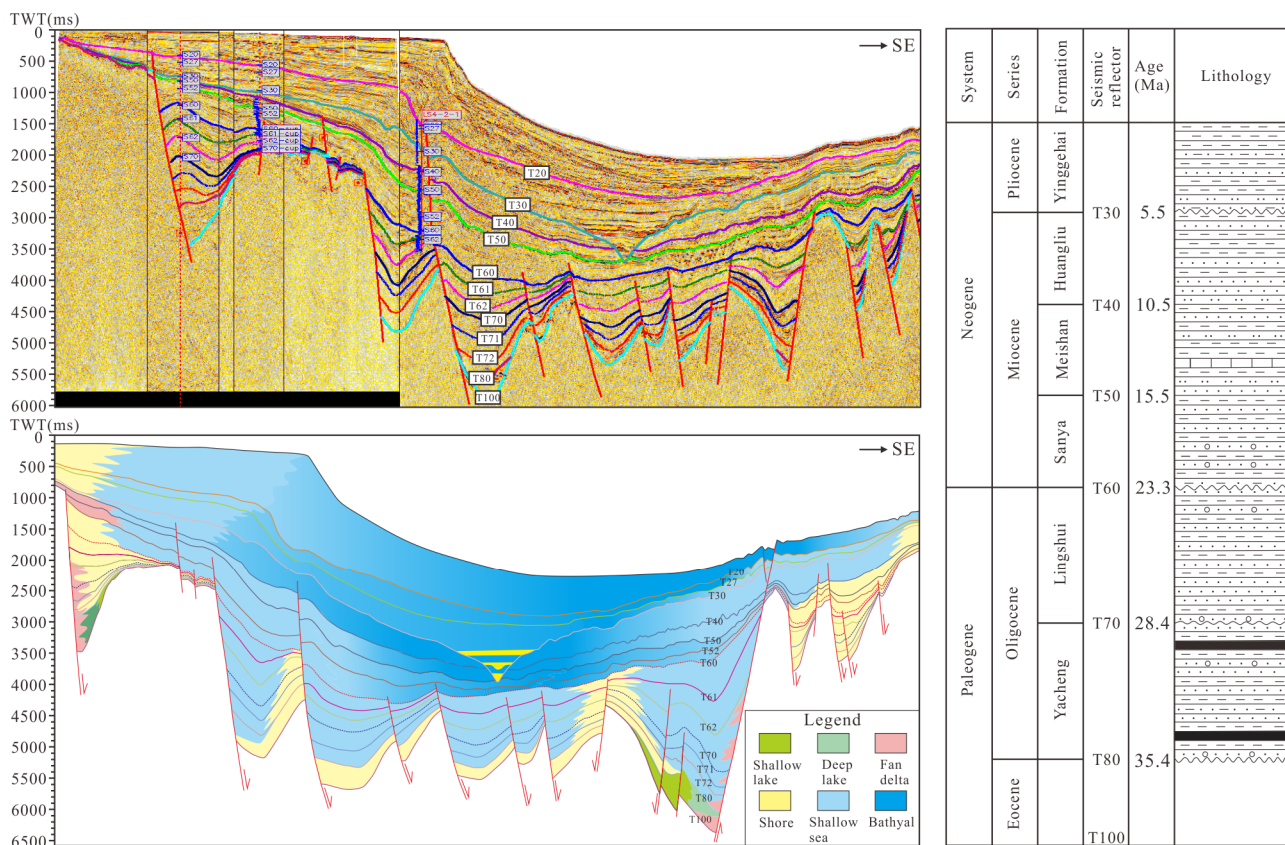


Figure 2. The left seismic profile and interpretation profile shows the internal structure, tectonic stage, sedimentary facies and evolution of the Qiongdongnan Basin. The right sketch map shows the sequence classification, seismic reflector, geologic age and lithologic characteristics of the Qiongdongnan Basin. The ages of the sequence boundaries and formations in the Qiongdongnan Basin were provided by the Research Institute of China National Offshore Oil Corporation.

3. Materials and Methods

3.1. Samples and Their Petrography, Porosity and Permeability

Systematic observations were conducted on cores from the QDNB, covering approximately 200 m of the cores from 10 wells. The China National Offshore Oil Corporation (CNOOC) provided 60 core samples from the MSF, SYF and LSF sandstone. Sixty samples were prepared as cast thin sections to investigate the mineralogical compositions, diagenesis and pores. A Nikon LV100 polarizing petrographic microscope (Nikon Corporation, Tokyo, Japan) was used to observe thin sections under different magnifications. Quantitative petrographic analysis was performed by counting at least 300 points/thin sections, to differentiate between detrital composition, cements, foraminifera and types of pores. Scanning electron microscope (SEM) analysis was performed on nineteen samples using an FEI Merlin Compact SEM (Carl Zeiss AG, Oberkochen, Germany). The purpose of the SEM analyses was to determine the type and morphology of the foraminifera. Approximately 406 mineralogical compositions of the MSF, SYF and LSF sandstone were used, of which 110 mineralogical compositions refer to different samples that were point-counted through thin sections, 162 mineralogical compositions were obtained from the CNOOC, and the other 134 mineralogical compositions from Gao [48] and Zhong [49]. Approximately 2438 porosity and permeability values of the LSF, SYF, MSF, HLF and YGHF sandstone were used, of which 1147 porosities and permeabilities were obtained from the CNOOC, and the other 1291 from Zhao [50], You [51] and Su [52,53].

3.2. The Lower Porosity and Permeability Limits of Effective Reservoir Analysis

The lower porosity and permeability limits of the effective reservoir were investigated using 423 measured porosities and permeabilities and interpreted gas saturations from 44 wells (including the prementioned 10 wells of which samples were prepared as cast thin sections to investigate the pores). Depending on whether the reservoir contains natural gas and water, the reservoirs were interpreted as a gas layer, gas and water layer, gas-bearing water layer, water layer and dry layer [13–15]. The CNOOC provided the porosity, permeability and gas- or water-layer interpretation results. Here, we define the gas-bearing water layer, gas and water layer, gas layer and water layer as the geological fluid-bearing layer. On the cross-plot with porosity and permeability as abscissa and ordinate, respectively, the samples of those interpreted as the dry layer are frequently distributed in different regions, with the samples interpreted as a geological fluid-bearing layer, and the porosity and permeability boundaries between them are considered as the lower porosity and permeability limits of the effective reservoir [13–15].

4. Results

4.1. Sandstone Petrography

4.1.1. Late Oligocene LSF

The LSF sandstone includes four lithofacies: conglomeratic coarse sandstone, coarse sandstone, fine sandstone and siltstone (see Figure 3). The LSF sandstone comprises subfeldsarenite, sublitharenite, litharenite, feldspathic litharenite, lithic arkose and feldsarenite (see Figure 4A). The average quartz content is 59.5%, of which the single-crystal quartz content is 45.9%, the polycrystalline quartz content is 13.6% and the secondary growth of quartz is generally developed (see Figure 5A). The average feldspar content is 16.3% and its type is primarily potassium feldspar. The average rock fragment content is 7.7% and the type is predominantly igneous and metamorphic rock fragments (see Figure 5A). The average matrix content is 10.4%, and the cement is dominated by calcite, with a content of 0.2–8.6%, followed by iron dolomite (3.5%) and iron calcite (2.1%). The grain size is typically fine to medium with a few coarse grains present, well-to-moderately sorted and subangular to round (see Figure 5A).

4.1.2. Lower Miocene SYF

The SYF sandstone includes two lithofacies, primarily comprising siltstone and fine sandstone (see Figure 3). The SYF sandstone contains subfeldsarenite and sublitharenite and some quartz arenite and litharenite (see Figure 4B). The average quartz, feldspar and rock fragment contents are 60.3%, 6.9% and 6.4%, respectively (see Figure 5B). The feldspar and rock fragments are mainly potassium feldspar and metamorphic and extrusive rock fragments, with average contents of 6.7%, 2.3% and 2.6%, respectively. The argillaceous matrix content is 2.7–34.6%. The cement is mainly iron calcite (avg. 4.5%), followed by dolomite (2.8%) and iron dolomite (2.8%). The grain size is silt to fine grain, poorly to moderately sorted and angular to subangular (see Figure 5B).

4.1.3. Middle Miocene MSF

The MSF sandstone includes two lithofacies, primarily comprising siltstone and muddy siltstone (see Figure 3). The MSF sandstone contains subfeldsarenite, sublitharenite, litharenite, feldspathic litharenite and some quartz arenite (see Figure 4C). The quartz content ranges from 33.0% to 74.0% (avg. 51.8%) (see Figure 5C). Quartz primarily comprises single-crystal quartz; the secondary growth of quartz is undeveloped. The feldspar content is 2.5–6.5% (avg. 5.5%) and its type is mainly potassium feldspar. The rock fragment content is 1.0–2.5% (avg. 1.6%) and the type is primarily metamorphic rock fragments (avg. 1.5%). The argillaceous matrix content in sandstone ranges from 2% to 26% (avg. 7.3%). The cement is mainly iron calcite (5.3%), followed by calcite (1.3%), dolomite (1.1%) and iron dolomite (0.6%). The sandstone texture of the MSF is similar to that of the SYF, with the silt grain size being poorly sorted and angular to subangular (see Figure 5C).

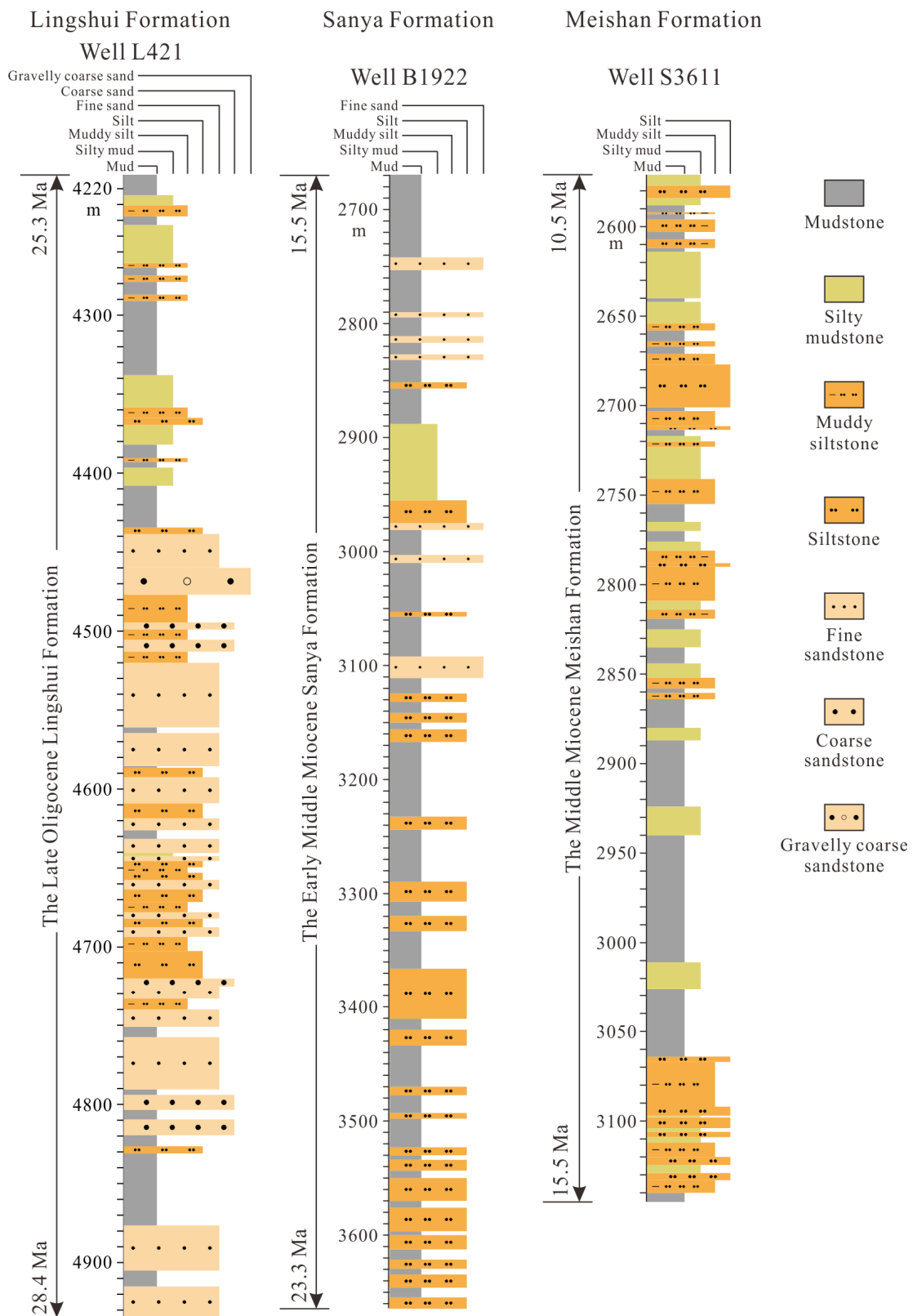


Figure 3. Well L421 shows that the Lingshui Formation sandstone comprises siltstone, fine sandstone, coarse sandstone and conglomeratic coarse sandstone; well B1922 shows that the Sanya Formation sandstone comprises siltstone and fine sandstone; and well S3611 shows that the Meishan Formation sandstone comprises siltstone and muddy siltstone.

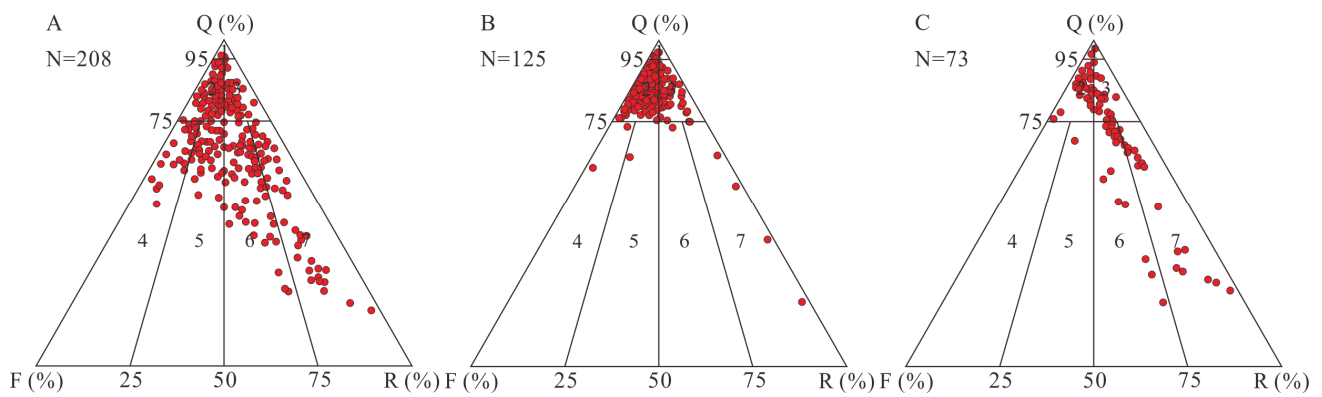


Figure 4. The mineralogical compositions of (A) the Lingshui Formation, (B) the Sanya Formation and (C) the Meishan Formation sandstones are plotted in the triangular chart (after Folk [54]). 1: quartz arenite; 2: subfeldsarenite; 3: sublitharenite; 4: feldsarenite; 5: lithic arkose; 6: feldspathic litharenite; 7: litharenite.

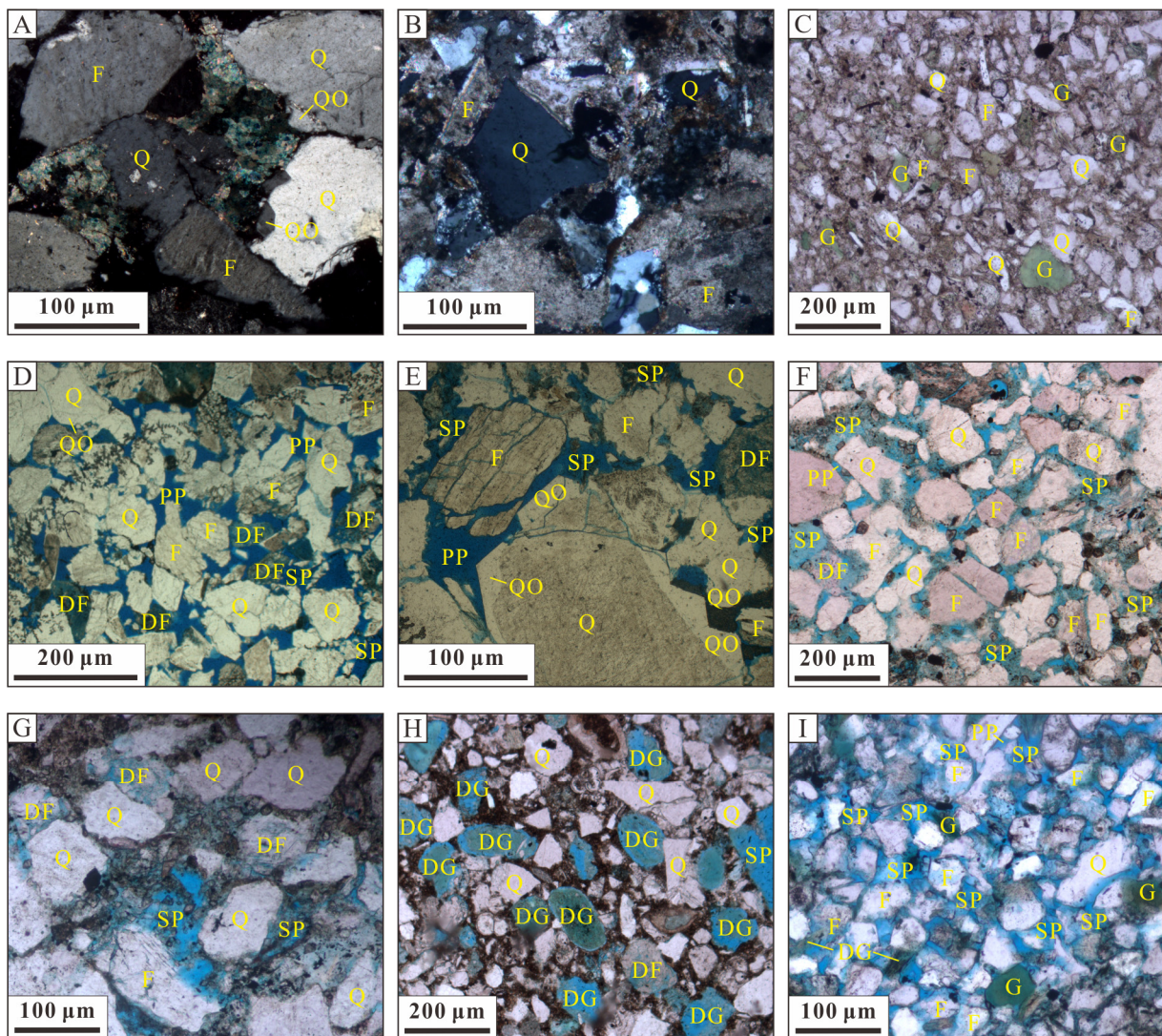


Figure 5. Lithology and pore characteristics of the Lingshui, Sanya and Meishan Formation sandstones. (A) The thin-section micrograph shows that the Lingshui Formation (LSF) sandstone is fine-medium grain, moderately well-sorted and subangular to subrounded; well Y1312, 3883.15 m.

(B) The Sanya Formation (SYF) sandstone is silt to fine grain, poorly to moderately sorted and angular to subangular; well S3431, 2575.20 m. (C) The Meishan Formation sandstone is silt grain, moderately sorted and angular to subangular; well B1923, 2426.50 m. (D) A few primary intergranular and many intergranular dissolution pores are developed in the LSF sandstone; well Y1921, 3827.90 m. (E) Feldspar grains dissolved to form intragranular pores in the LSF sandstone; well Y1313, 3816.10 m. (F) Secondary dissolution pores are widely developed in the SYF sandstone; well S3431, 2576.00 m. (G) Feldspar grains dissolved to form intragranular pores in the SYF sandstone; well S3431, 2572.90 m. (H) Glauconite grains dissolved to form intergranular and intragranular pores in the SYF sandstone; Well S3431, 2566.00 m. (I) Secondary dissolution pores are widely developed in the Meishan Formation sandstone; well B1311, 1582.10 m. Legend: quartz (Q), quartz overgrowth (QO), feldspar (F), dissolved feldspar (DF), glauconite (G), dissolved glauconite (DG), primary porosity (PP), secondary pores (SP).

4.2. Pore Systems

4.2.1. Primary Intergranular Pore

Only a few primary intergranular pores are preserved in the LSF, SYF and MSF sandstones. The minerals are typically inline or in uneven contact because the LSF sandstone has undergone strong compaction (see Figure 5A). The lesser development of cement allows a few primary intergranular pores to be retained (see Figure 5D,E). These pores are usually triangular or elongated in thin sections. The SYF and MSF sandstones experience inadequate compaction and the minerals are typically in point contact (see Figure 5F–I). Because of strong carbonate cementation and the generous argillaceous filling, the primary intergranular pores in the SYF and MSF sandstones were not preserved. Only when the MSF sandstone is well-sorted and the argillaceous matrix is low can the residual primary intergranular pores be observed between the quartz grains.

4.2.2. Secondary Dissolution Pore

Secondary dissolution pores widely exist in the LSF, SYF and MSF sandstones (see Figure 5E–I). The dissolution pores comprise intergranular dissolved, intragranular dissolved, mould and dissolution-enlarged pores (see Figure 5E–I).

The intergranular dissolution pores in the LSF, SYF and MSF sandstones are primarily formed by the dissolution of the feldspar grain edges (see Figure 5E,F,I). The morphology of the feldspar intergranular dissolution pores is highly irregular, frequently showing a bay-like shape. Furthermore, the intergranular dissolution pores related to the dissolution of the glauconite grain edges are developed in the SYF and MSF sandstones (see Figure 5H,I). Since glauconite is a unique mineral in the SYF and MSF sandstones, the intergranular dissolution pores related to glauconite are unique to the SYF and MSF sandstones (see Figure 5H,I). The morphology of glauconite intergranular dissolution pores is much more regular than that of feldspar intergranular dissolution pores, frequently similar to the shape of the glauconite particles (see Figure 5H).

The feldspar and glauconite intragranular dissolution primarily form the intragranular dissolution pores in the LSF, SYF and MSF sandstones (see Figure 5E,G,H). The intragranular dissolution of feldspar is widespread in the LSF sandstone (see Figure 5E). However, the intragranular dissolution of glauconite is more common in the SYF and MSF sandstones (see Figure 5H). The intragranular dissolution pores related to glauconite in the SYF and MSF sandstones are more developed than the intergranular dissolution pores related to feldspar. Feldspar intragranular dissolution is frequently carried along the cleavage of feldspar to the periphery to form irregular intragranular dissolution pores (see Figure 5E). The dissolution pores in glauconite grains are primarily regular, continuous flakes (see Figure 5H).

Mould pores are widely developed in the SYF and MSF sandstones and are formed when the glauconite particle is almost entirely dissolved, and only the outline of the grain remains (see Figure 5H). The size and shape of the glauconite grains determine the size and morphology of these pores. The glauconite in the SYF and MSF sandstones are

mainly stripes, triangles and ellipses; therefore, the related mould pores are also stripes, triangles and ellipses. The complete dissolution of feldspar to form a mould pore is rarely observed. However, after several continuously arranged feldspars undergo intergranular or intragranular dissolution, dissolution-enlarged pores are formed in the LSF, SYF and MSF sandstones.

4.2.3. Foraminiferal Cavities

Foraminifera are widely developed in the SYF sandstone and are occasionally observed in the MSF sandstone (see Figure 6). The most common foraminifera in the SYF sandstone are in the *Operculina* sp. It contains a few fossil fragments of the *Cycloclypeus* sp. and *Miogypsina* sp., with a shell diameter of 2–6 mm (see Figure 6). Other biological debris included minimal *Globigerina* and bivalves. Foraminiferal shells in thin sections typically appear in a directional arrangement. The size of foraminiferal bodies buried in the same position is similar, the shells are intact and many foraminiferal cavities are preserved. Foraminiferal cavities are isolated pores separated by partition walls, and only some are partially connected due to the destruction of the shell structure (see Figure 6).

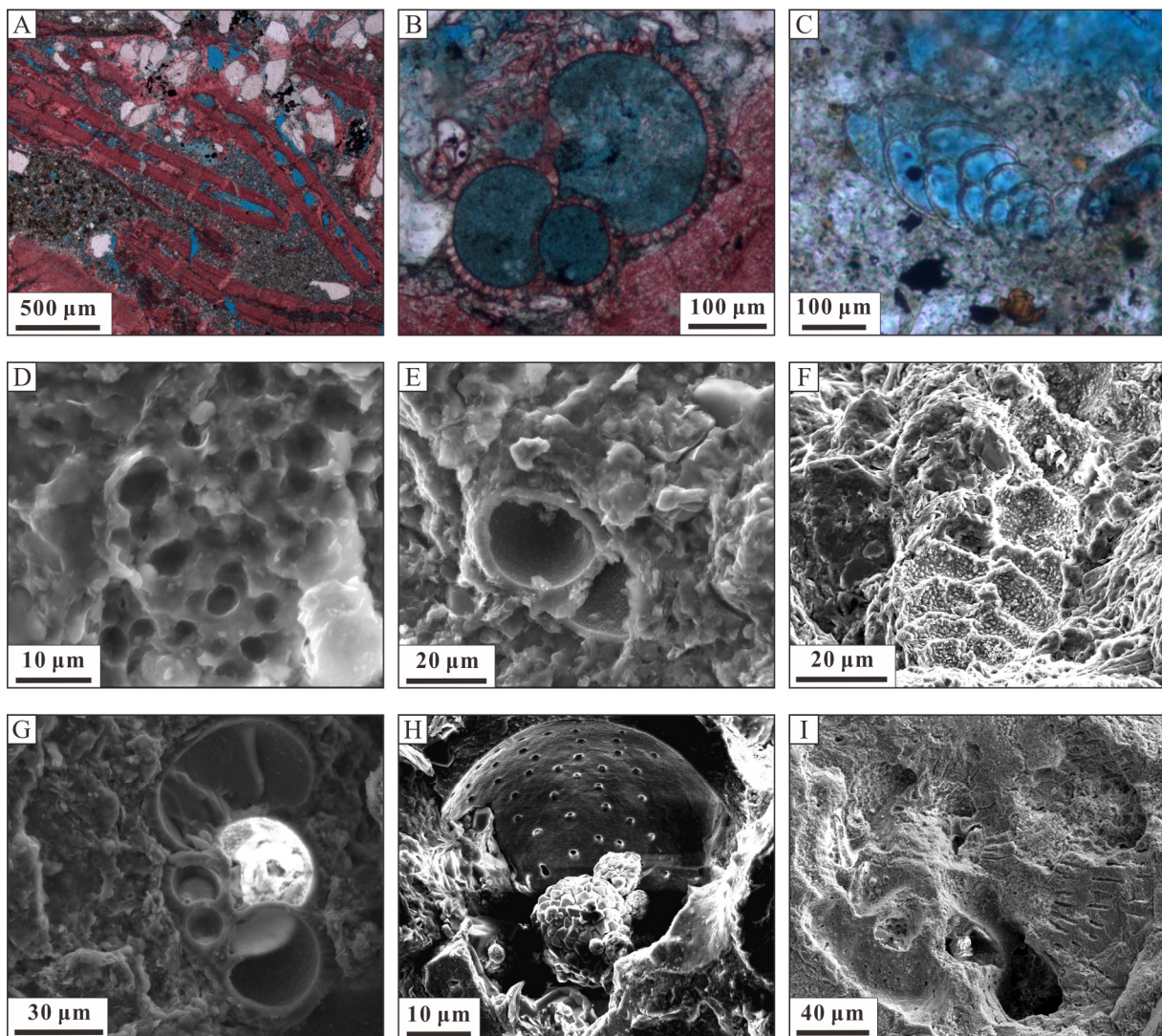


Figure 6. (A–C) Thin-section micrographs and (D–I) SEM images showing pores in various foraminiferal cavities. (A) The chambers in orientated foraminifera were well preserved, well S3431, 2570.90 m. (B) Spherical chambers in foraminifera, well S3431, 2568.10 m. (C) The chambers in foraminifera were well preserved, well S3611, 3257.80 m. (D) The pores in the outer wall of foraminifera,

well S3611, 3257.80 m. (E) Spherical chambers in foraminifera, well S3611, 3257.80 m. (F) The chambers in foraminifera, well S3611, 2813.20 m. (G) Spherical chambers in foraminifera, well S3611, 3257.80 m. (H) The pores in the outer wall of foraminifera, well B1331, 1968.90 m. (I) The chambers in foraminifera, well Y9, 2221.57 m.

4.3. Porosity and Permeability

In the western QDNB, the LSF sandstone has a porosity of 2.1–29.35% and a permeability of $0.07\text{--}2549 \times 10^{-3} \mu\text{m}^2$ (see Figure 7A,B). Three abnormally high petrophysical property zones developed at depths of 2700–2900 m, 3650–4150 m and 4450–4800 m with maximum porosities of approximately 30%, 25% and 20%, respectively (see Figure 7A). In the eastern QDNB, the amount of LSF sandstone with a burial depth of less than 3500 m porosity is generally high, ranging from 10% to 30%, and that of LSF with a burial depth greater than 3500 m is rapidly reduced to 2–15% (see Figure 7A). Two abnormally high porosity zones developed at depths of 3750–4300 m and 4800–5250 m, with maximum porosities of approximately 17% and 13% (see Figure 7A).

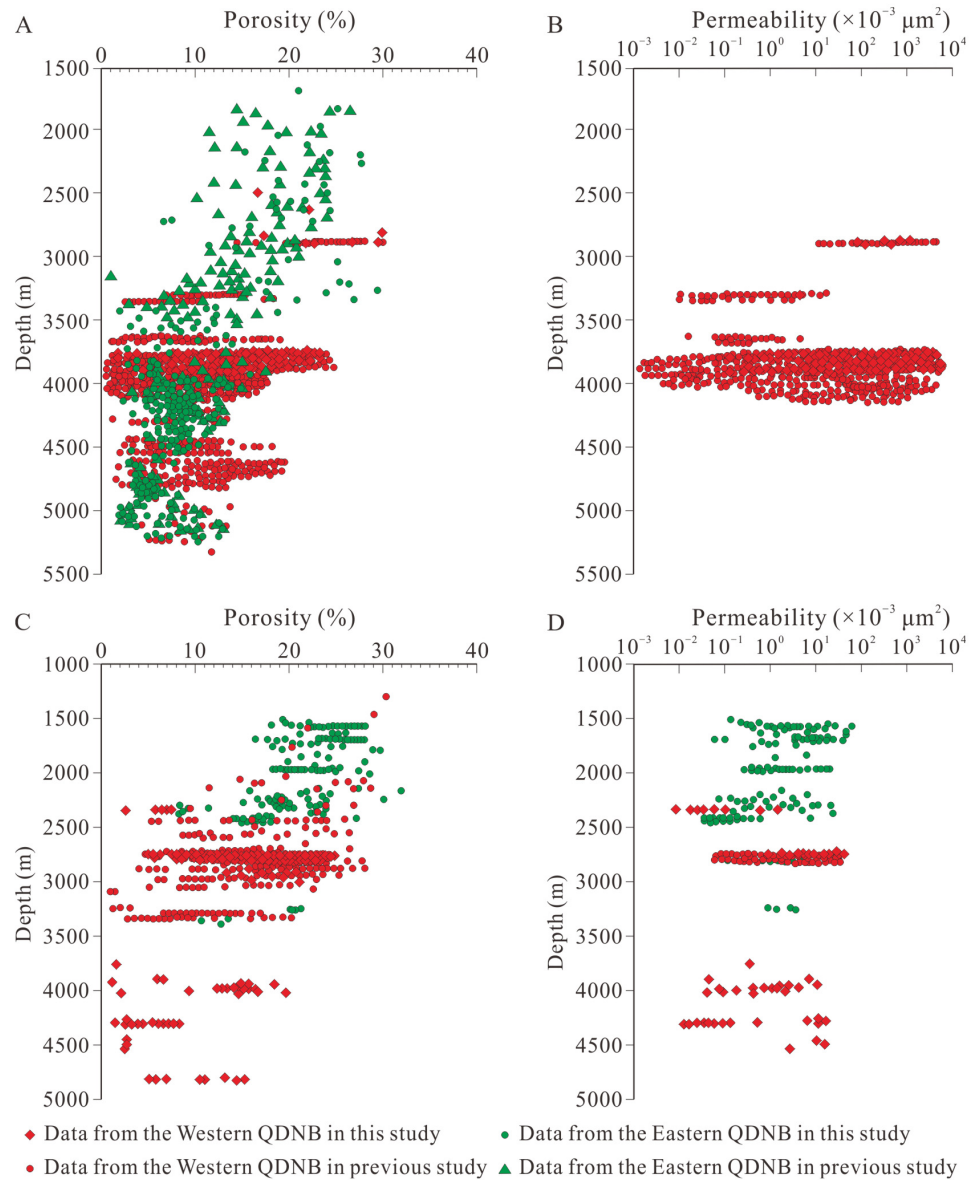


Figure 7. (A) Porosity and (B) permeability of the Lingshui Formation sandstones. (C) Porosity and (D) permeability of the Sanya and Meishan Formation sandstones.

The burial depths of the SYF and MSF sandstones in the western QDNB are typically greater (>2300 m) than those in the eastern QDNB. The burial depth of the SYF and MSF sandstones in the western QDNB is generally greater than 2300 m, whereas that of the eastern QDNB is usually less than 2500 m. The difference in the SYF and MSF sandstones' burial depths in the eastern QDNB ensures a higher porosity of 8–32% and permeability of $0.05\text{--}93.8 \times 10^{-3} \mu\text{m}^2$, whereas, in the western QDNB, they have a low porosity of 1–28% and permeability of $0.01\text{--}20 \times 10^{-3} \mu\text{m}^2$ (see Figure 7C,D). The SYF and MSF sandstones in the western QDNB developed one abnormally high porosity zone at 4700–4800 m deep (see Figure 7C).

5. Discussion

5.1. The Lower Porosity and Permeability Limits of the Effective Reservoir

5.1.1. Sandstone in Different Sedimentary Facies

Various sedimentary facies are developed in the QDNB, including delta, submarine canyon and submarine fan [35,40,42,46]. The lower porosity and permeability limits of effective reservoirs in different sedimentary facies is an exciting topic. Considering that the submarine fan data are few in this study, the submarine fan and submarine canyon data are taken as the sample for statistical analysis. Statistical analysis shows that the porosity and permeability of sandstone developed in the delta are greater than 8.9% and $1.2 \times 10^{-3} \mu\text{m}^2$, respectively, and the sandstone might contain water or natural gas, thus becoming an effective reservoir (see Figure 8A). For sandstone developed in submarine canyons and fans, the lower porosity and permeability limits of sandstone that can become an effective reservoir are 11.3% and $4.0 \times 10^{-3} \mu\text{m}^2$, respectively (see Figure 8B). The result indicates that with the increase in the sediment transport distance, the lower porosity and permeability limits of the reservoir will increase. The possible reason for this result is that, with the increase in the sediment transport distance, the sandstone will be better sorted and rounded. Intergranular pore development is more common, resulting in the sandstone having higher porosity and permeability. When geological fluids enter these sandstone layers, they preferentially accumulate into a reservoir with higher porosity and permeability. This process improves the lower porosity and permeability limits of whether the sandstone can contain geological fluids.

5.1.2. Sandstone with Different Grain Sizes

Argillaceous siltstone, siltstone and fine and coarse sandstone are enriched in the QDNB [40–42]. The pore structures and petrophysical parameters of sandstone with different grain sizes vary considerably [49–53]. Therefore, it is necessary to analyse the lower porosity and permeability limits of effective reservoirs with varying grain sizes. Statistical analysis shows that only when the porosity and permeability of coarse sandstone, fine sandstone, siltstone and argillaceous siltstone are greater than 9.9% and $7.7 \times 10^{-3} \mu\text{m}^2$, 10.2% and $1.9 \times 10^{-3} \mu\text{m}^2$, 12.3% and $9.9 \times 10^{-3} \mu\text{m}^2$ and 12.2% and $3.9 \times 10^{-3} \mu\text{m}^2$, respectively (see Figure 8C–F), the sandstone might contain water or natural gas, thus becoming effective reservoirs. The result indicates that with the decreasing grain size, the lower porosity limit for sandstone to be an effective reservoir will increase and no significant correlation exists between the grain size and lower permeability limit because, with the decrease in grain size, the porosity and permeability of the reservoir decrease. It is challenging for geological fluids to enter reservoir with poor porosity and permeability, requiring higher porosity and permeability limits for siltstones to be effective reservoirs.

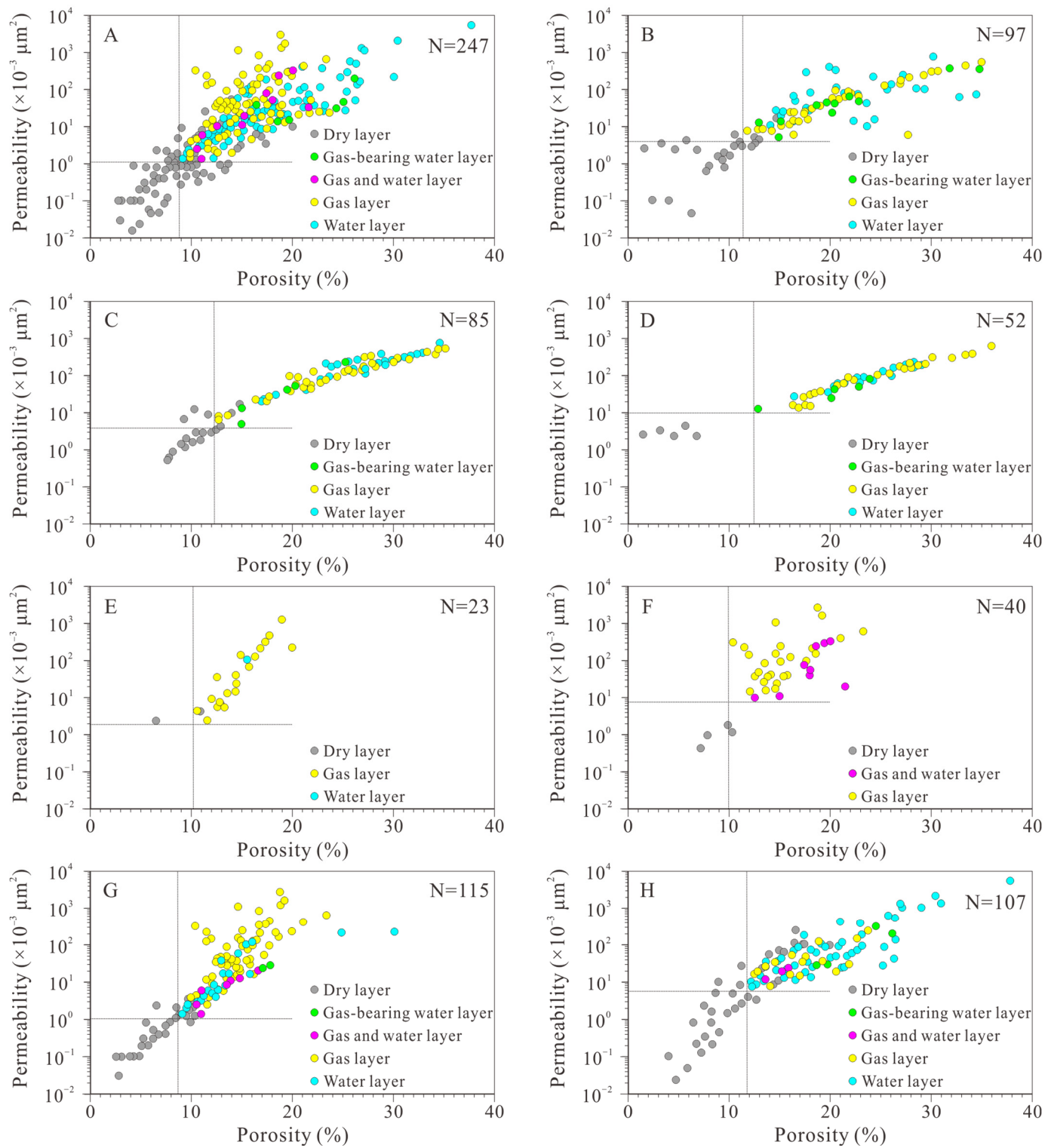


Figure 8. The porosity, permeability and gas testing relation graphs of the sandstones developed in the (A) deltas, (B) submarine canyons and fans, (C) coarse sandstone, (D) fine sandstone, (E) siltstone, (F) argillaceous siltstone, (G) Lingshui Formation and (H) Sanya and Meishan formations.

5.1.3. Sandstone in Different Strata

The burial depth of the sandstone influences its diagenetic process, which will change the petrophysical parameters of the sandstone, causing the reservoir in the deep stratum to frequently have a lower porosity and permeability [49–51,55]. We discuss the variation in

the lower porosity and permeability limits of effective reservoirs in different formations. Considering the small thickness and few data of the MSF (primarily 100–250 m thick), the MSF and the SYF data are taken as samples for statistics. Statistical analysis shows that the porosity and permeability of sandstone developed in the late Oligocene LSF are greater than 8.8% and $1.0 \times 10^{-3} \mu\text{m}^2$, respectively, and the sandstone might contain water or natural gas, thus becoming an effective reservoir (see Figure 8G). For sandstone developed in the Miocene MSF and SYF, the lower porosity and permeability limits of sandstone that can become effective reservoirs are 11.8% and $5.7 \times 10^{-3} \mu\text{m}^2$ (see Figure 8H). The result indicates that with the decrease in the stratum period, the lower porosity and permeability limits of the effective reservoir will increase because, in shallower buried formations, sandstone tends to experience weaker compaction and cementation, resulting in higher porosity and permeability. When geological fluids enter the shallower buried sandstone, they preferentially accumulate into sandstone with high porosity and permeability. This process improves the lower porosity and permeability limits of whether the shallower buried sandstone can contain geological fluids.

5.2. Formation Mechanism of the Effective Reservoir

5.2.1. Effect of Sediment Source and Transport Distance

Sediment source and transport distance are fundamental factors determining the petrophysical parameters of the QDNB sandstone [41,49,51]. In particular, the sediment transport distance significantly influences the petrophysical parameters of sandstones [41,49,50]. A petrophysical parameter comparative analysis shows that the sandstone sourced from the Red River drainage has experienced the longest transport distance [42,45,46], and the porosity and permeability are the highest (see Figure 9A). The sandstone reservoir sourced from the Hainan Uplift experienced a medium transport distance [34,36,44], and the porosity and permeability are in the middle of the three provenances (see Figure 9A). The sandstone reservoir sourced from the palaeo-uplift within the basin experienced the shortest transport distance [41], and the porosity and permeability were minor in the three provenances (see Figure 9A). Furthermore, the petrophysical parameters of sandstones from the palaeo-uplift within the QDNB and the Hainan Uplift vary widely, indicating that only a portion of the sandstone from these two provenances can be effective reservoirs (see Figure 9A).

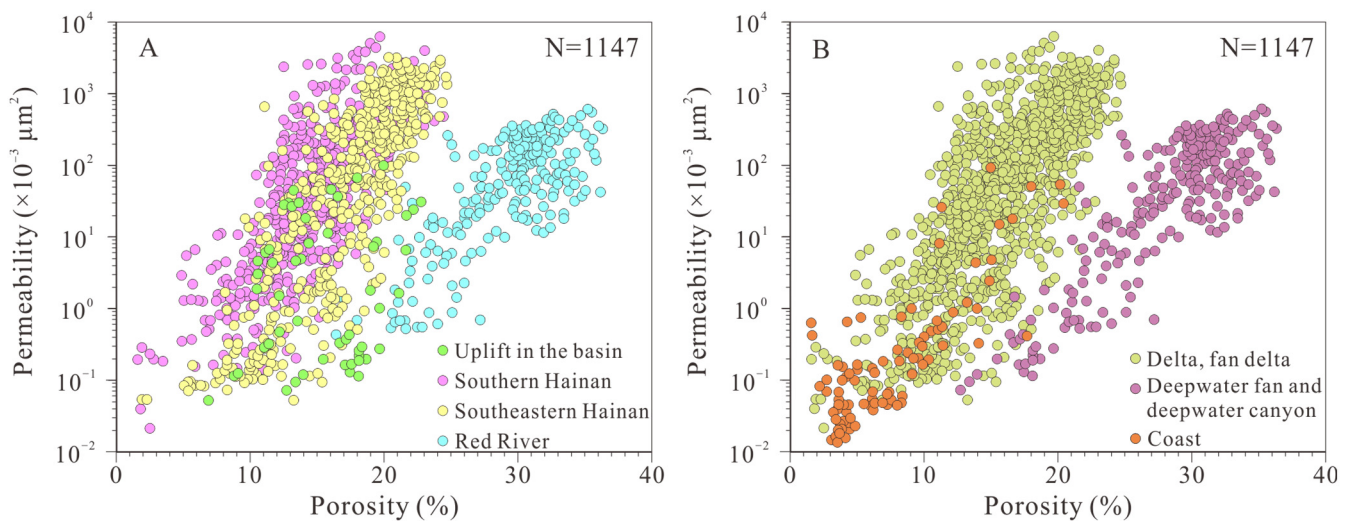


Figure 9. The relationship between porosity, permeability and (A) sediment source and (B) sedimentary facies of the sandstones in the Qiongdongnan Basin.

5.2.2. Effect of Sedimentary Facies

Reservoir quality is influenced by depositional process [55] and sedimentary facies are therefore another major factor determining the petrophysical parameters of the QDNB sandstone [49–51]. A comparative analysis of the petrophysical parameters of sandstone

developed in different sedimentary facies shows that the sandstones developed in deep-water fans and submarine canyons have higher porosity and permeability, followed by deltas and fan deltas. The sandstone developed in the coastal area has the lowest porosity and permeability (see Figure 9B). The porosity and permeability of sandstone developed in deepwater fans, submarine canyons, fan deltas and deltas of the QDNB vary widely. The deepwater sedimentary sandstone sourced from the Red River system has higher porosity and permeability, whereas that from the southeast Hainan Uplift has a lower porosity and permeability (see Figure 9). The sandstones developed in fan deltas and deltas have a wide range of porosity and permeability because the sediment sources are primarily from the palaeo-uplift within the basin and the Hainan Uplift (see Figure 9).

5.2.3. Dissolution of Various Minerals during Diagenesis

(1) Dissolved minerals

Feldspar dissolution is an important diagenetic reaction affecting reservoir quality evolution in sandstones with detrital feldspars [56]. Feldspar particles are the primary dissolved minerals in the LSF sandstone reservoir of the QDNB (see Figure 5D,E). The average feldspar content in the LSF sandstone is 16.3%, of which 85% have suffered varying degrees of dissolution. Some feldspar particles are only dissolved at the outer edge, and some are inside the particles (see Figure 5D,E). Most feldspar particles in the LSF sandstone were dissolved, indicating that the feldspar content determines the development degree of dissolution pores. The feldspar content in the LSF sandstone is proportional to the grain size of the sandstone [48,49]. In sandstone reservoirs with coarser grain sizes, the feldspar content is higher and the dissolution pores of feldspar are more developed than those with finer grain sizes [48,49].

In addition to feldspar, glauconite dissolution is more common in the SYF and MSF sandstone reservoirs (see Figure 5H). The average feldspar contents in the SYF and MSF sandstone reservoirs are 6.9% and 5.5%, respectively, which is much lower than the feldspar content in the LSF sandstone reservoir. However, the glauconite content in the SYF and MSF sandstone reservoirs reached 3–15%, of which 95% have suffered different degrees of dissolution (see Figure 5H). Moreover, most dissolution occurs inside the glauconite particles, which significantly contributed to the dissolution pore development in the SYF and MSF sandstones (see Figure 5H).

(2) Dissolved acidic geological fluids

Carbonic acid is one of the primary acidic fluids in the QDNB [57]. The CO₂ content in the natural gas reservoir of the QDNB is 0.5–97.2%, and, in particular the CO₂ content in the natural gas reservoir distributed in the northern SN–BDS is typically higher than 80% [53,58]. The carbon isotope value of CO₂ in the QDNB is between −7.50‰ and 3.90‰, the value of ³He/⁴He is 3.46–8.75 × 10^{−6} and the R/Ra value is between 2.47 and 7.87 [53,58]. Such recorded values indicates that the CO₂ in the QDNB is primarily of mantle-derived inorganic origin. Mantle-derived CO₂ in the QDNB enters sandstone reservoirs mainly through magmatic diapirs and eruptive volcanoes [58]. The fluid inclusions show that the CO₂ charging periods are the Pliocene and Quaternary [53,58]. Simulation experiments show that CO₂-rich deionised water can have a strong dissolution effect on potash feldspar and albite [57].

The organic acid released from the source rock is another essential acidic fluid in the QDNB [53]. The source rocks in the QDNB are developed in the YCF [58]. The YCF in shallow-water areas comprises 483–910 m mudstones and 5–13.5 m carbonaceous mudstones and coals [58]. The total organic carbon (TOC) value is 0.4–98.5% [58]. The YCF in deepwater areas comprises shales, carbonaceous shales and coals, with TOC values of 0.4–21% [58]. The YCF source rocks primarily contain types IIb and III kerogens [58]. The YCF source rocks in the QDNB reached a mature stage at 22 Ma and entered the gas generation window at 10 Ma [58]. Thermal simulation experiments show that the YCF source rocks can generate many organic acids, with an average yield ratio of organic acid to

kerogen of 3.8 mg/g; moreover, the primary component is oxalic acid, which has a strong dissolution ability [53]. When the organic acids generated by the YCF source rocks enter the adjacent sandstone reservoir of the LSF, SYF and MSF along the fault system, they dissolve the soluble minerals in the sandstone reservoir and form dissolution pores [56].

5.3. Implication for Deepwater Natural Gas Exploration

The LSF effective reservoir in the deepwater area of the QDNB is mainly distributed in the northern margin of the LDS and LSS, the periphery of the SNU and the northern margin of the SNS. The sedimentary facies of the sand bodies in the northern area of the LDS and LSS are deepwater fans [41]. The sediments of these deepwater fans are mainly sourced from the deltas developed in the Yacheng area, where the sediments are primarily medium- and coarse-grained sandstone [41]. Therefore, deepwater fan sandstone developed in the northern margin of the LDS and LSS is also considered coarse grained [41]. Furthermore, dissolution pores are widely developed in the LSF sandstone in this area. The facies of the sand body developed on the periphery of the SNU is a beach bar, and no drilling has encountered this set of sand bodies. From the sedimentary environment, it is inferred that the sandstone should be pure. It is adjacent to the source rock and prone to organic acid dissolution. The sedimentary facies of the sand bodies developed in the northern margin of the SNS are fan deltas and coastal seas and are prone to organic acid dissolution.

The SYF effective reservoir in the deepwater area of the QDNB is mainly distributed in the northern margin of the LDS and LSS. The sedimentary facies of the sand bodies developed in the northern margin of the LDS and LSS are deepwater fans [41]. However, the grain size and argillaceous content of the sandstone vary [41]. The delta sediments developed on the northern shelf of the LDS and LSS have a coarse grain size, making the deepwater fans developed in this area have a coarser grain size and lower argillaceous content than in other areas [41]. Furthermore, the development of dissolution pores results in the deepwater fan sand bodies in this area having a higher porosity and permeability.

The MSF effective reservoir in the deepwater area of the QDNB is primarily distributed in the central and northern regions of the LDS and LSS and the northern margin of the SNS and CCS. The depositional facies of the sandstone are deepwater fans [40]. The sand bodies developed in the LDS and LSS are sheet sand but differ from the sheet sand in the northern margin of the SNS [40]. The sheet sand developed in the northern area of the LDS and LSS has a coarser grain size and lower argillaceous content [40]. Simultaneously, due to the development of dissolution pores, the sheet sand developed in the LDS and LSS has high porosity and permeability. The sheet sand developed in the northern margin of the SNS has multiple stages of evolution [40]. The deepwater fans developed in the early stage are small, are dominated by siltstone and rich in argillaceous [40]. The deepwater fans developed when the sea level decreased to the lowest during the middle Miocene has a large scale and a fine grain size [40]. Moreover, no magmatic diapirs are developed in the development area of the late-stage deepwater fan, which can avoid CO₂ filling [57]. The sedimentary facies of the sand bodies developed in the northern margin of the CCS are deepwater channels [40]. The lithology of the deepwater channel sandstone is well-sorted fine sandstone [40] with a high porosity and permeability.

6. Conclusions

This study analysed the lower petrophysical property limits and their influence factors of the effective marine sandstone gas reservoirs in the Qiongdongnan Basin using porosity, permeability and gas testing. Then, the roles of sediment source, sediment transport distance, sedimentary facies and dissolution diagenesis on the formation of an effective sandstone reservoir were evaluated, and finally the favourable reservoir development zone was proposed.

- A few primary intergranular and many secondary dissolution pores are preserved in the LSF, SYF and MSF sandstones of the QDNB. Foraminifera were widely preserved in the SYF sandstone. In the western QDNB, three abnormally high porosity

and permeability zones developed in the LSF at depths of 2700–2900 m, 3650–4150 m and 4450–4800 m, whereas there are two abnormally high porosity zones in the eastern QDNB at depths of 3750–4300 m and 4800–5250 m. The SYF and MSF sandstones in the eastern QDNB have a high porosity of 8–32% and a permeability of $0.05\text{--}93.8 \times 10^{-3} \mu\text{m}^2$, whereas the SYF and MSF sandstones in the western QDNB have a low porosity of 1–28% and a permeability of $0.01\text{--}20 \times 10^{-3} \mu\text{m}^2$. The SYF and MSF sandstones in the western QDNB developed abnormally high porosity at 4700–4800 m deep.

- The lower porosity and permeability limits of effective reservoirs developed in the deltas are 8.9% and $1.2 \times 10^{-3} \mu\text{m}^2$, whereas the lower porosity and permeability limits of those developed in submarine canyons and fans are 11.3% and $4.0 \times 10^{-3} \mu\text{m}^2$. The lower porosity and permeability limits of the effective reservoirs with coarse, fine, silty and argillaceous silty grain sizes are 9.9% and $7.7 \times 10^{-3} \mu\text{m}^2$, 10.2% and $1.9 \times 10^{-3} \mu\text{m}^2$, 12.3% and $9.9 \times 10^{-3} \mu\text{m}^2$ and 12.2% and $3.9 \times 10^{-3} \mu\text{m}^2$, respectively. The lower porosity and permeability limits of effective reservoirs developed in the late Oligocene LSF are 8.8% and $1.0 \times 10^{-3} \mu\text{m}^2$, whereas the lower porosity and permeability limits of effective reservoirs developed in the Miocene MSF and SYF are 11.8% and $5.7 \times 10^{-3} \mu\text{m}^2$.
- The sandstones from the Red River have higher porosity and permeability, followed by those from the Hainan Uplift. The palaeo-uplift within the basin presents the lowest porosity and permeability. The sandstone reservoirs developed in deepwater fans and submarine canyons have a higher porosity and permeability, followed by deltas and fan deltas, and the sandstone reservoir developed in coastal areas has the lowest porosity and permeability. Dissolution of the feldspars by CO_2 and organic acid, resulting in dissolution pores, is considered the primary mechanism for increased porosity of the effective LSF reservoir. Glauconite particle dissolution is common in the SYF and MSF sandstone reservoirs.

Author Contributions: Conceptualization, C.L. and G.C.; methodology, C.L. and S.G.; formal analysis, C.L. and C.X.; resources, S.G.; writing—original draft preparation, C.L.; writing—review and editing, Q.Z.; visualization, C.X.; funding acquisition, G.C. All authors have read and agreed to the published version of the manuscript.

Funding: This research was funded by “Youth Innovation Promotion Association CAS” (Grant No. 2022431), and the National Science and Technology Major Project of the Ministry of Science and Technology of China (Grant No. 2016ZX05026-007-05).

Institutional Review Board Statement: Not applicable.

Informed Consent Statement: Not applicable.

Data Availability Statement: The data that support the findings of this study are available within the article.

Acknowledgments: We are grateful to the Research Institute of the China National Offshore Oil Corporation for their technical support, sampling assistance and granting permission to publish the results of this study.

Conflicts of Interest: Author S.G. was employed by the Research Institute of China National Offshore Oil Corporation. The remaining authors declare that the research was conducted in the absence of any commercial or financial relationships that could be construed as a potential conflict of interest.

References

1. Behmanesh, H.; Hamdi, H.; Clarkson, C.R.; Thompson, J.M.; Anderson, D.M. Analytical modeling of linear flow in single-phase tight oil and tight gas reservoirs. *J. Pet. Sci. Eng.* **2018**, *171*, 1084–1098. [[CrossRef](#)]
2. Hu, S.Y.; Zhu, R.K.; Wu, S.T.; Bai, B.; Yang, Z.; Cui, J.W. Exploration and development of continental tight oil in China. *Pet. Explor. Dev.* **2018**, *45*, 790–802. [[CrossRef](#)]

3. Milad, M.; Junin, R.; Sidek, A.; Imqam, A.; Alusta, G.A.; Augustine, A.; Abdulazeez, M.A. Experimental investigation of bypassed-oil recovery in tight reservoir rock using a two-step CO₂ soaking strategy: Effects of fracture geometry. *Upstream Oil Gas Technol.* **2023**, *11*, 100093. [[CrossRef](#)]
4. Sun, L.D.; Zou, C.N.; Jia, A.L.; Wei, Y.S.; Zhu, R.K.; Wu, S.T.; Guo, Z. Development characteristics and orientation of tight oil and gas in China. *Pet. Explor. Dev.* **2019**, *46*, 1073–1087. [[CrossRef](#)]
5. Syed, F.I.; Dhaghi, A.K.; Muther, T. Laboratory to field scale assessment for EOR applicability in tight oil reservoirs. *Pet. Sci.* **2022**, *19*, 2131–2149. [[CrossRef](#)]
6. Meng, M.M.; Zhang, Y.X.; Yuan, B.; Li, Z.J.; Zhang, Y. Imbibition behavior of oil-saturated rock: Implications for enhanced oil recovery in unconventional reservoirs. *Energy Fuels* **2023**, *37*, 13759–13768. [[CrossRef](#)]
7. Altawati, F.; Emadi, H.; Pathak, S. Improving oil recovery of Eagle Ford shale samples using cryogenic and cyclic gas injection methods—An experimental study. *Fuel* **2021**, *302*, 121170. [[CrossRef](#)]
8. Du, J.H.; Liu, H.; Ma, D.S.; Fu, J.H.; Wang, Y.H.; Zhou, T.Y. Discussion on effective development techniques for continental tight oil in China. *Pet. Explor. Dev.* **2014**, *41*, 217–224. [[CrossRef](#)]
9. Lange, S.S.; Shrestha, L.; Nnoli, N.; Aniagu, S.; Rawat, S.; McCant, D. Do shale oil and gas production activities impact ambient air quality? A comprehensive study of 12 years of chemical concentrations and well production data from the Barnett Shale region of Texas. *Environ. Int.* **2023**, *175*, 107930. [[CrossRef](#)]
10. Solarin, S.A.; Gil-Alana, L.A.; Lafuente, C. An investigation of long range reliance on shale oil and shale gas production in the U.S. market. *Energy* **2020**, *195*, 116933. [[CrossRef](#)]
11. Wang, H.; Liao, X.; Lu, N.; Cai, Z.; Liao, C.; Dou, X. A study on development effect of horizontal well with SRV in unconventional tight oil reservoir. *J. Energy Inst.* **2014**, *87*, 114–120. [[CrossRef](#)]
12. Wei, J.G.; Zhou, X.F.; Zhou, J.M.; Li, J.T.; Wang, A.L. Recovery efficiency of tight oil reservoirs with different injection fluids: An experimental investigation of oil-water distribution feature. *J. Pet. Sci. Eng.* **2020**, *195*, 107678. [[CrossRef](#)]
13. Bai, Y.B.; Zhao, J.Z.; Wu, W.T. Methods to determine the upper limits of petrophysical properties in tight oil reservoirs: Examples from the Ordos and Songliao Basins. *J. Pet. Sci. Eng.* **2021**, *196*, 107983. [[CrossRef](#)]
14. Cui, H.Y.; Zhong, N.N.; Li, J.; Wang, D.L.; Li, Z.S.; Hao, A.S.; Liang, F. Study on the lower limits of petrophysical parameters of the Upper Paleozoic tight sandstone gas reservoirs in the Ordos Basin, China. *J. Nat. Gas Geosci.* **2017**, *2*, 21–28. [[CrossRef](#)]
15. Pang, H.; Ding, X.G.; Pang, X.Q.; Geng, H. Lower limits of petrophysical parameters allowing tight oil accumulation in the Lucaogou Formation, Jimusaer Depression, Junggar Basin, Western China. *Mar. Pet. Geol.* **2019**, *101*, 428–439. [[CrossRef](#)]
16. Shakya, S.; Li, B.X.; Etienne, X.L. Shale revolution, oil and gas prices, and drilling activities in the United States. *Energy Econ.* **2022**, *108*, 105877. [[CrossRef](#)]
17. Zheng, D.Y.; Pang, X.Q.; Zhou, L.M.; You, X.C.; Liu, X.H.; Guo, F.X.; Li, W. Critical conditions of tight oil charging and determination of the lower limits of petrophysical properties for effective tight reservoirs: A case study from the Fengcheng Formation in the Fengcheng area, Junggar Basin. *J. Pet. Sci. Eng.* **2020**, *190*, 107135. [[CrossRef](#)]
18. Qiao, J.C.; Zeng, J.H.; Cai, J.C.; Jiang, S.; An, T.; Xiao, E.Z.; Zhang, Y.C.; Feng, X.; Yang, G.Q. Pore-scale heterogeneity of tight gas sandstone: Origins and impacts. *J. Nat. Gas Sci. Eng.* **2021**, *96*, 104248. [[CrossRef](#)]
19. Šliaupa, S.; Lozovskis, S.; Lazauskienė, J.; Šliaupienė, R. Petrophysical and mechanical properties of the lower Silurian perspective oil/gas shales of Lithuania. *J. Nat. Gas Sci. Eng.* **2020**, *79*, 103336. [[CrossRef](#)]
20. Wang, J.; Cao, Y.C.; Xiao, J.; Liu, K.Y.; Song, M.S. Factors controlling reservoir properties and hydrocarbon accumulation of the Eocene lacustrine beach-bar sandstones in the Dongying Depression, Bohai Bay Basin, China. *Mar. Pet. Geol.* **2019**, *99*, 1–16. [[CrossRef](#)]
21. Zhang, F.; Jiang, Z.X.; Sun, W.; Li, Y.H.; Zhang, X.; Zhu, L.; Wen, M. A multiscale comprehensive study on pore structure of tight sandstone reservoir realized by nuclear magnetic resonance, high pressure mercury injection and constant-rate mercury injection penetration test. *Mar. Pet. Geol.* **2019**, *109*, 208–222. [[CrossRef](#)]
22. Zhang, L.C.; Song, X.J.; Du, Y.J.; Lu, S.F.; Xiao, D.S.; Jiang, S.; Chen, X.L.; Zhang, R.; Yu, R.Y. The upper and lower limits and grading evaluation of the Shahezi tight gas reservoirs in the Xujiaweizi Rift, northern Songliao Basin: Implications from microscopic pore structures. *J. Pet. Sci. Eng.* **2022**, *212*, 110224. [[CrossRef](#)]
23. Randolph, M.F.; Gaudin, C.; Gourvenec, S.M.; White, D.J.; Boylan, N.; Cassidy, M.J. Recent advances in offshore geotechnics for deep water oil and gas developments. *Ocean Eng.* **2011**, *38*, 818–834. [[CrossRef](#)]
24. Skogdalen, J.E.; Vinnem, J.E. Quantitative risk analysis of oil and gas drilling, using Deepwater Horizon as case study. *Reliab. Eng. Syst. Saf.* **2012**, *100*, 58–66. [[CrossRef](#)]
25. Huo, J.H.; Zhang, R.Z.; Yu, B.S.; Che, Y.J.; Wu, Z.S.; Zhang, X.; Peng, Z.G. Preparation, characterization, investigation of phase change micro-encapsulated thermal control material used for energy storage and temperature regulation in deep-water oil and gas development. *Energy* **2022**, *239*, 122342. [[CrossRef](#)]
26. Epuh, E.E.; Joshua, E.O. Modeling of porosity and permeability for hydrocarbon Exploration: A case study of Gongola arm of the Upper Benue Trough. *J. Afr. Earth Sci.* **2020**, *162*, 103646. [[CrossRef](#)]
27. Farahani, M.; Aghaei, H.; Masoumi, H. Effect of pore type on porosity, permeability and pore volume compressibility of geological formations due to in-situ stress change. *J. Pet. Sci. Eng.* **2022**, *218*, 110986. [[CrossRef](#)]

28. Wang, J.J.; Wu, S.H.; Li, Q.; Zhang, J.J.; Guo, Q.H. Characterization of the pore-throat size of tight oil reservoirs and its control on reservoir physical properties: A case study of the Triassic tight sandstone of the sediment gravity flow in the Ordos Basin, China. *J. Pet. Sci. Eng.* **2020**, *186*, 106701. [[CrossRef](#)]
29. Xia, Y.X.; Tian, Z.H.; Xu, S.; Wei, W.; Cai, J.C. Effects of microstructural and petrophysical properties on spontaneous imbibition in tight sandstone reservoirs. *J. Nat. Gas Sci. Eng.* **2021**, *96*, 104225. [[CrossRef](#)]
30. Meng, M.; Ge, H.; Shen, Y.; Ji, W.; Wang, Q. Rock fabric of tight sandstone and its influence on irreducible water saturation in Eastern Ordos Basin. *Energy Fuels* **2023**, *37*, 3685–3696. [[CrossRef](#)]
31. Er, C.; Zhao, J.Z.; Li, Y.Y.; Si, S.H.; Bai, Y.B.; Wu, W.T.; Han, Q.Y. Relationship between tight reservoir diagenesis and hydrocarbon accumulation: An example from the early Cretaceous Fuyu reservoir in the Daqing oil field, Songliao Basin, China. *J. Pet. Sci. Eng.* **2022**, *208*, 109422. [[CrossRef](#)]
32. Liu, K.; Wang, R.; Shi, W.Z.; Zhang, W.; Qi, R.; Qin, S.; Xu, L.T. Tectonic controls on Permian tight gas accumulation: Constrains from fluid inclusion and paleo-structure reconstruction in the Hangjinqi area, northern Ordos Basin, China. *J. Nat. Gas Sci. Eng.* **2020**, *83*, 103616. [[CrossRef](#)]
33. Ren, D.Z.; Zhou, D.S.; Liu, D.K.; Dong, F.J.; Ma, S.W.; Huang, H. Formation mechanism of the Upper Triassic Yanchang Formation tight sandstone reservoir in Ordos Basin—Take Chang 6 reservoir in Jiyuan oil field as an example. *J. Pet. Sci. Eng.* **2019**, *178*, 497–505. [[CrossRef](#)]
34. Hu, B.; Wang, L.S.; Yan, W.B.; Liu, S.W.; Cai, D.S.; Zhang, G.C.; Zhong, K.; Pei, J.X.; Sun, B. The tectonic evolution of the Qiongdongnan Basin in the northern margin of the South China Sea. *J. Asian Earth Sci.* **2013**, *77*, 163–182. [[CrossRef](#)]
35. Franke, D.; Savva, D.; Pubellier, M.; Steuer, S.; Mouly, B.; Auxietre, J.-L.; Meresse, F.; Chamot-Rooke, N. The final rifting evolution in the South China Sea. *Mar. Pet. Geol.* **2014**, *58*, 704–720. [[CrossRef](#)]
36. Morley, C.K. Major unconformities/termination of extension events and associated surfaces in the South China Seas: Review and implications for tectonic development. *J. Asian Earth Sci.* **2016**, *120*, 62–86. [[CrossRef](#)]
37. Gong, C.L.; Wang, Y.M.; Hodgson, D.M.; Zhu, W.L.; Li, W.G.; Xu, Q.; Li, D. Origin and anatomy of two different types of mass-transport complexes: A 3D seismic case study from the northern South China Sea margin. *Mar. Pet. Geol.* **2014**, *54*, 198–215. [[CrossRef](#)]
38. Wang, Z.F.; Sun, Z.P.; Zhang, D.J.; Zhu, J.T.; Li, X.S.; Huang, B.J.; Guo, M.G.; Jiang, R.F. Geology and hydrocarbon accumulations in the deepwater of the northwestern South China Sea—With focus on natural gas. *Acta Oceanol. Sin.* **2015**, *34*, 57–70. [[CrossRef](#)]
39. Clift, P.D.; Carter, A.; Wysocka, A.; Van Hoang, L.; Zheng, H.; Neubeck, N. A Late Eocene–Oligocene through-flowing River between the Upper Yangtze and South China Sea. *Geochem. Geophys. Geosystems* **2020**, *21*, e2020GC009046. [[CrossRef](#)]
40. Li, C.; Chen, G.J.; Zhou, Q.S.; Yang, H.Z.; Lyu, C.F.; Guo, S.; Sun, R.; Ma, M. Seismic geomorphology of three types of deepwater fans and their relationship with slope morphology: Qiongdongnan Basin, northern South China Sea. *Mar. Pet. Geol.* **2021**, *124*, 104814. [[CrossRef](#)]
41. Lyu, C.F.; Li, C.; Chen, G.J.; Zhang, G.C.; Ma, M.; Zhang, Y.; Sun, Z.T.; Zhou, Q.S. Zircon U–Pb age constraints on the provenance of Upper Oligocene to Upper Miocene sandstones in the western Qiongdongnan Basin, South China sea. *Mar. Pet. Geol.* **2021**, *126*, 104891. [[CrossRef](#)]
42. Wang, Y.M.; Xu, Q.; Li, D.; Han, J.H.; Lü, M.; Wang, Y.F.; Li, W.G.; Wang, H.R. Late Miocene red river submarine fan, northwestern South China Sea. *Chin. Sci. Bull.* **2011**, *56*, 1488–1494. [[CrossRef](#)]
43. Zhao, M.; Shao, L.; Liang, J.S.; Li, Q.Y. No Red River capture since the late Oligocene: Geochemical evidence from the Northwestern South China Sea. *Deep. Sea Res. Part II Top. Stud. Oceanogr.* **2015**, *122*, 185–194. [[CrossRef](#)]
44. Savva, D.; Pubellier, M.; Franke, D.; Chamot-Rooke, N.; Meresse, F.; Steuer, S.; Auxietre, J.L. Different expressions of rifting on the South China Sea margins. *Mar. Pet. Geol.* **2014**, *58*, 579–598. [[CrossRef](#)]
45. Liang, C.; Liu, C.Y.; Xie, X.N.; Yu, X.H.; He, Y.L.; Chen, H.; Zhou, Z.; Tian, D.M.; Lu, B.Y.; Mi, H.G.; et al. The role of large-scale mass wasting processes in changing the sediment dispersal pattern in the deep-water Central Canyon of the northwestern South China Sea. *Mar. Pet. Geol.* **2020**, *122*, 104693. [[CrossRef](#)]
46. Su, M.; Wu, C.H.; Chen, H.; Li, D.F.; Jiang, T.; Xie, X.N.; Jiao, H.J.; Wang, Z.F.; Sun, X.M. Late Miocene provenance evolution at the head of Central Canyon in the Qiongdongnan Basin, Northern South China Sea. *Mar. Pet. Geol.* **2019**, *110*, 787–796. [[CrossRef](#)]
47. Yang, S.; Qiu, Y.; Zhu, B. *Atlas of Geology and Geophysics of the South China Sea*; China Navigation Publications: Tianjin, China, 2015.
48. Gao, Y.; Qu, X.Y.; Yang, X.B.; You, L.; Zhong, J.; Dong, X.F.; Cao, Y.Q.; Wang, Y.P. Characteristics of fluid inclusions and accumulation period of Miocene reservoir in Ledong-Lingshui Sag of Qiongdongnan Basin. *Mar. Orig. Pet. Geol.* **2018**, *23*, 83–90. (In Chinese with English Abstract)
49. Zhong, J.; Yang, X.B.; Zhu, P.Y.; Xu, S.L.; Deng, X.L.; Tuo, L.; Li, X.; Song, P. Porosity evolution differences of the Lingshui Formation reservoir between Baodao and Changchang Sag, Qiongdongnan Basin. *Earth Sci.* **2019**, *44*, 2665–2676. (In Chinese with English Abstract)
50. Zhao, X.Q. *Diagenesis and the Favourable Reservoir Prediction of the Target Layer in the Qiongdongnan Basin*; Northeast Petroleum University: Daqing, China, 2010. (In Chinese with English Abstract)
51. You, L.; Li, W.; Li, C.; Zhao, Z.J. Main factors affecting physical properties of deep burial reservoir in Baodao area of Southeast Hainan Basin. *Spec. Oil Gas Reserv.* **2014**, *21*, 37–40. (In Chinese with English Abstract)

52. Su, A.; Chen, H.H.; He, C.; Lei, C.; Lei, M.Z.; Liu, Y.H. Diagenesis controlling development of abnormal high porosity zones: A case from Yacheng area in the western Qiongdongnan basin, South China Sea. *J. China University Min. Technol.* **2017**, *46*, 345–355. (In Chinese with English Abstract)
53. Su, A.; Du, J.M.; Chen, H.H.; Yu, Y.; Lei, M.Z. Diagenetic fluid type and activity history of controlling the development of abnormal pore zone: Taking the north margin of Baodao Sag, Qiongdongnan Basin as an example. *Nat. Gas Geosci.* **2016**, *27*, 1837–1847. (In Chinese with English Abstract)
54. Folk, R.L. *Petrology of Sedimentary Rocks*; Hemphills Publishing Company: Sutton, UK, 1974.
55. Sun, N.L.; Zhong, J.H.; Ge, Y.Z.; van Loon, A.T. Reservoir quality of the Middle-Late Triassic Yanchang Formation (Ordos Basin) as controlled by sedimentology and diagenesis. In *The Ordos Basin*; Elsevier: Amsterdam, The Netherlands, 2022; pp. 421–460.
56. Yuan, G.H.; Cao, Y.C.; Gluyas, J.; Xiaoyan, L.; Xi, K.L.; Wang, Y.Z.; Jia, Z.Z.; Sun, P.; Oxtoby, N. Feldspar dissolution, authigenic clays, and quartz cements in open and closed sandstone geochemical systems during diagenesis: Typical examples from two sags in Bohai Bay Basin, East China. *AAPG Bull.* **2015**, *99*, 2121–2154. [[CrossRef](#)]
57. Li, C.Z.; Chen, G.J.; Li, C.; Tian, B.; Sun, R.; Su, L.; Lu, Y.X.; Wang, L.J. Experimental Study on Water-rock Reactions with CO₂ Fluid in a Deep Sandstone Formation under High Temperature and Pressure. *Acta Geol. Sin.-Engl. Ed.* **2021**, *95*, 268–279. [[CrossRef](#)]
58. Huang, B.J.; Tian, H.; Li, X.S.; Wang, Z.F.; Xiao, X.M. Geochemistry, origin and accumulation of natural gases in the deepwater area of the Qiongdongnan Basin, South China Sea. *Mar. Pet. Geol.* **2016**, *72*, 254–267. [[CrossRef](#)]

Disclaimer/Publisher’s Note: The statements, opinions and data contained in all publications are solely those of the individual author(s) and contributor(s) and not of MDPI and/or the editor(s). MDPI and/or the editor(s) disclaim responsibility for any injury to people or property resulting from any ideas, methods, instructions or products referred to in the content.